# A theoretical assessment of the feasibility of potential Lunar Reconnaissance Orbiter radio occultation observations of the lunar ionosphere

Paul Withers,[a,b,*] T. J. Stubbs,[c] E. Mazarico[c]

[a] *Department of Astronomy, Boston University, 725 Commonwealth Avenue, Boston, MA 02215, USA*

[b] *Center for Space Physics, Boston University, 725 Commonwealth Avenue, Boston, MA 02215, USA*

[c] *NASA Goddard Space Flight Center, Greenbelt, MD, USA.*

**Abstract**

The existence of a "dense" lunar ionosphere has been controversial for decades. Positive ions produced from the lunar surface and exosphere are inferred to have densities that are $\lesssim 10^6$ – $10^7$ m$^{-3}$ near the surface and smaller at higher altitudes, yet electron densities derived from radio occultation measurements occasionally exceed these values by orders of magnitude. For example, about 4% of the single-spacecraft radio occultation measurements from Kaguya/SELENE were consistent with peak electron densities of $\sim 3 \times 10^8$ m$^{-3}$. Space plasmas should be neutral on macroscopic scales, so this represents a substantial discrepancy. Aditional observations of electron densities in the lunar ionosphere are critical to resolving this longstanding paradox. Here we theoretically assess whether radio occultation obser-

vations using two-way coherent S-band radio signals from the Lunar Reconnaissance Orbiter (LRO) spacecraft could provide useful measurements of electron densities in the lunar ionosphere. We predict the uncertainty in a single LRO radio occultation measurement of electron density to be $\sim 3 \times 10^8$ m$^{-3}$, comparable to occasional observations by Kaguya/SELENE of a dense lunar ionosphere. Thus an individual profile from LRO is unlikely to reliably detect the lunar ionosphere; however, averages of multiple ($\sim$10) LRO profiles acquired under similar geophysical and viewing conditions should be able to make reliable detections. An observing rate of six ingress occultations per day ($\sim$2000 per year) could be achieved with minimal impact on current LRO operations. This rate compares favorably with the 378 observations reported from the single-spacecraft experiment on Kaguya/SELENE between November 2007 and June 2009. The large number of observations possible for LRO would be sufficient to permit wide-ranging investigations of spatial and temporal variations in the poorly understood lunar ionosphere. These findings strengthen efforts to conduct such observations with LRO.

*Key words:* Radio occultation, ionosphere, Moon

## 1 Introduction

The Moon is surrounded by a tenuous neutral atmosphere (Stern, 1999). At all altitudes, neutral number densities are so low that collisions are rare. In other atmospheres, this condition occurs only above the high-altitude exobase (Chamberlain and Hunten, 1987; Catling and Kasting, 2017). Consequently, the lunar atmosphere can be described as a surface-bounded exosphere. It

* Corresponding author
*Email address:* withers@bu.edu (Paul Withers,).

lacks the thermosphere, stratosphere, and troposphere regions familiar in the atmospheres of many larger solar system objects.

In general, a thermosphere in a solar system atmosphere contains a weakly-ionized plasma derived from the ionization of thermospheric neutrals. This is called an ionosphere. An ionosphere is an important part of the boundary between a solar system object and the surrounding space environment. It participates in the exchange of mass, momentum, and energy between the solar system object and the space environment. Its properties reflect the properties of the neutral atmosphere from which the ionosphere is derived and also reflect the physical processes by which the magnetically-controlled space environment interacts with the gravitationally-controlled neutral atmosphere. An ionosphere participates in atmospheric loss processes; it is both a reservoir from which escape occurs and a pathway through which neutral particles are converted into ions that can escape more readily. From a mission operations perspective, an ionosphere impacts radio communication and navigation systems. These considerations are valid at the Moon. The lunar ionosphere will play a role in the interactions between the solar wind and the solid surface of the Moon. The lunar ionosphere will be intimately associated with the neutral atmosphere and volatile species that exchange readily between surface and atmosphere, such as mission-enabling water. Hence efforts to characterize the state of the lunar ionosphere and determine the processes that shape it contribute to wider efforts to understand the origin and evolution of the Moon.

As the Moon lacks a traditional thermosphere, it will not have a traditional ionosphere. It is instead surrounded by a region of highly tenuous, lunar-derived plasma, which is also referred to as an ionosphere (Stern, 1999). However, the existence of a "dense" lunar ionosphere is controversial as present

ionospheric observations are confusing and contradictory (e.g., Stubbs, 2018).

Direct measurements of the densities of positive ions near the Moon are not available (e.g., Stern, 1999). Fluxes, but not densities, of ions were measured by the Suprathermal Ion Detector Experiment (SIDE) emplaced by Apollo 12, 14, and 15 (Benson et al., 1975) and the Charged Particle Lunar Environment Experiment (CPLEE) emplaced by Apollo 14 (Reasoner and O'Brien, 1972; Reasoner and Burke, 1972). The largest fluxes observed regularly by SIDE were $\sim 10^5$ cm$^{-2}$ s$^{-1}$ sr$^{-1}$; these occurred at local sunrise/sunset (Stern, 1999). Based on these ion flux measurements and neutral atmospheric density measurements, positive ions produced from the lunar surface and exosphere are inferred to have densities that are $\lesssim 10^6$ – $10^7$ m$^{-3}$ near the surface and smaller at higher altitudes (Vondrak, 1992; Stern, 1999; Stubbs et al., 2011; Stubbs, 2018), yet electron densities derived from radio occultation measurements can occasionally exceed these values by orders of magnitude. For example, about 4% of the single-spacecraft radio occultation measurements from the Kaguya spacecraft (also known as SELENE, SELenological and ENgineering Explorer spacecraft) were consistent with peak electron densities of $\sim 3 \times 10^8$ m$^{-3}$ (Imamura et al., 2012). Measurement uncertainties were $\sim 1 \times 10^8$ m$^{-3}$. These observations were acquired from November 2007 to June 2009. Their latitude and solar zenith angle coverage is reported in Figure 1 of Imamura et al. (2012). Yet the net charge density of plasma in a solar system ionosphere is invariably zero (Cravens, 2004). That is, the plasma is neutral. If it is not, then the resultant strong electric fields accelerate mobile electrons to re-establish neutrality. Violations of neutrality are not permitted on lengthscales longer than the Debye shielding length, which is much smaller than the characteristic lengthscales of solar system ionospheres. However, current observations of ion

densities of $\lesssim 10^6$ – $10^7$ $m^{-3}$ and electron densities of $\sim 3 \times 10^8$ $m^{-3}$, if taken at face value, improbably suggest that the lunar ionosphere severely violates the strong expectation of neutrality. This paradox has not yet been resolved.

The primary challenge is to explain the sporadic observations of large values of electron density. Over the past five decades, there have been scarcely two dozen possible radio occultation detections of a dense lunar ionosphere using spacecraft in lunar orbit (Stubbs, 2018). Therefore, the acquisition of additional observations is essential to solve the puzzle of the state of the lunar ionosphere.

Radio occultation observations by the Lunar Reconnaissance Orbiter (LRO) spacecraft may be able to provide useful measurements of electron densities in the lunar ionosphere. The aim of this article is to assess theoretically whether such measurements are feasible.

The structure of this article is as follows. Section 2 introduces the lunar ionosphere. Section 3 introduces the radio occultation method. Section 4 introduces the radio science capabilities of the LRO spacecraft. Section 5 presents examples of LRO radio tracking data. Section 6 describes the methods used to generate synthetic ionospheric electron density profiles from LRO radio tracking data. Section 7 presents the set of synthetic ionospheric electron density profiles. Section 8 interprets the characteristics of these synthetic ionospheric electron density profiles. Section 9 presents the conclusions of this work.

## 2 The lunar ionosphere

The lunar exosphere contains gases released from the solid body of the Moon by outgassing, meteoroid impacts, sputtering by the solar wind, and photon-stimulated desorption. Due to its low density, it can be noticeably enhanced by outgassing from spacecraft that have landed on or impacted into the Moon. Exospheric species are photoionized by sunlight to produce ions and electrons, which are then picked up by the solar wind's electromagnetic fields and removed from the exosphere. Loss of these pickup ions occurs either by impact with the lunar surface or escape to space, and represents the dominant loss mechanism for most lunar exospheric neutral species.

Apollo instruments on the lunar surface detected fluxes of ion species inferred to be $Ne^+$ and $Ar^+$ (Stern, 1999, and references therein) (Stubbs, 2018, and references therein). Since the 1990s, ion mass spectrometers and related instruments on orbiters near the Moon have confirmed the presence of these ion species and detected a range of other ion species (Stubbs, 2018). Overall, these measurements of positive ions are consistent with ion production by ionization of neutral species in the lunar exosphere and with maximum ion densities $\lesssim 10^6$–$10^7$ $m^{-3}$ (Stern, 1999).

A very different picture is obtained from radio occultation experiments sensitive only to electrons, not ions or other charge carriers — a technique regularly used to measure electron density profiles in solar system ionospheres (e.g., Withers, 2010). Radio occultation experiments on Luna 19, Luna 22 (USSR), SMART-1 (ESA), Chandrayaan-1 (India), and Kaguya/SELENE (Japan) have occasionally inferred the presence of larger electron densities.

Though variable, the characteristic structure in such observations is that electron density values decrease exponentially with altitude with scale height ∼15 km and are ∼$3\times10^8$ $m^{-3}$ near the surface (Vasilev et al., 1974; Vyshlov, 1976; Pluchino et al., 2008; Choudhary et al., 2016; Ando et al., 2012; Imamura et al., 2012). However, such large values of electron density are infrequent (Stubbs, 2018). Only about 4% of the single-spacecraft radio occultation measurements from Kaguya/SELENE were consistent with large electron densities (Imamura et al., 2012). In most ionospheric electron density profiles acquired at the Moon by radio occultation experiments, electron densities are not significant relative to the experimental uncertainty, which is generally no better than ∼$1\times10^8$ $m^{-3}$. Overall, these measurements of electrons are consistent with an appreciable lunar ionosphere that occurs preferentially on the sunlit side of the Moon and is either spatially localized, episodic, or both (Imamura et al., 2012; Stubbs, 2018).

As discussed in Section 1, the small positive ion density measurements (Vondrak, 1992; Stern, 1999; Stubbs et al., 2011; Stubbs, 2018), sporadic large electron density measurements (Imamura et al., 2012), and the well-founded expectation of neutrality (Cravens, 2004) are not consistent. Several hypotheses have been proposed to resolve this dilemma. Savich (1976) suggested that electrons and ions could be trapped in regions of closed magnetic field lines and thereby protected against loss by solar wind pickup. However, Ando et al. (2012) compared electron density measurements from Luna 19, Luna 22, and Kaguya/SELENE dual spacecraft observations to modern maps of crustal magnetic field strength. They did not find correlations between locations of high electron density and locations of strong magnetic field. Furthermore, Stubbs et al. (2011) suggested that uncertainties affecting the calculations of

Savich (1976) could have caused these calculations of large trapped electron densities to be significant overestimates. Bauer (1996) suggested that photoemission of electrons from the lunar surface could cause large electron densities, but other authors noted that this population of electrons would have a scale height on the order of meters, not the required kilometers (Stubbs et al., 2011). Choudhary et al. (2016) suggested that the lunar ionosphere is composed primarily of molecular ions and is similar to a cometary ionosphere. Using a photochemical ionospheric model, they predicted near-surface electron densities on the order of $3\times10^8$ m$^{-3}$. However, these predicted density values relied on the adoption of atypically large values for the densities of neutral exospheric species. If more widely-accepted neutral density values are used, then predicted electron densities are significantly smaller (Stubbs, 2018).

Imamura et al. (2008) and Stubbs et al. (2011) suggested that small positive ion densities and large electron densities could be reconciled by invoking the presence of positively-charged dust in the lunar exosphere. Neither ion nor electron measurements would be sensitive to positively-charged dust. A handful of Apollo-era observations have indicated the occasional presence of high abundances of submicron exospheric dust with scale heights of order 10 km (McCoy, 1976), (Glenar et al., 2011), (Stubbs et al., 2011, and references therein). Moreover, the dust content varies episodically, which could be consistent with production from meteoroid impacts of modest size. This could explain why detections of large ionospheric electron densities occur sporadically. On the sunlit side of the Moon, dust grains exposed to solar ultraviolet radiation emit photoelectrons. Stubbs et al. (2011) estimated that electron densities on the order of $3\times10^8$ m$^{-3}$ could be produced by this mechanism. This could explain why detections of large ionospheric electron densities occur

preferentially on the sunlit side of the Moon.

The total number of robust radio occultation detections of electrons in the lunar ionosphere is surprisingly small. Vasilev et al. (1974) and Vyshlov (1976) presented six detections from 31 sets of observations by Luna 19 and 22, giving an occurrence rate of ∼20%. Pluchino et al. (2008) did not show any convincing detections from SMART-1. Choudhary et al. (2016) described only one detection from an undisclosed number of observations by Chandrayaan-1. Imamura et al. (2012) reported 16 detections from the 378 single-spacecraft observations of Kaguya/SELENE, giving only a ∼4% occurrence rate. Ando et al. (2012) reported 2 detections from the 19 dual-spacecraft observations of Kaguya/SELENE, giving a ∼10% occurrence rate. This total of only 25 spacecraft radio occultation detections of the lunar ionosphere — an occurrence rate of <6% at best — is clearly insufficient to characterize the spatial and temporal variability in the electron density distribution. In fact, prior to the Kaguya/SELENE results, it could be argued that all previously-reported claims of electron densities greater than $1{\times}10^8$ $m^{-3}$ were spurious.

## 3 Radio occultation methods for studying electron densities

The measurements of electron density in the lunar ionosphere that are described in Section 2 were acquired by radio occultation investigations. With the radio occultation method, vertical profiles of ionospheric electron density are obtained from time series measurements of the frequency of a radio signal. Specifically, of a radio signal that propagates between a spacecraft and Earth such that the ray path passes through the lunar ionosphere. The observing geometry is illustrated in Figure 1. The presence of dispersive free

electrons along the line of sight slightly bends the ray path (e.g., Withers et al., 2014) and affects the frequency of the radio signal (e.g., Phipps et al., 2018). Consequently, the received frequency is slightly different from its expected value, which is based upon the relativistic Doppler shift caused by the known motions of the spacecraft and ground station. The difference between the observed value of the received frequency and the expected value of the received frequency is known as the "frequency residual". Given knowledge of the trajectories of the relevant spacecraft, ground station, and target object (i.e., the Moon), standard procedures can be used to determine a vertical profile of ionosphere electron density from a time series of frequency residuals (e.g., Withers et al., 2014, and references therein).

## 4 Radio science capabilities of Lunar Reconnaissance Orbiter

LRO arrived at the Moon in June 2009 and entered into a circular polar orbit with an altitude of 50 km. The three main objectives of LRO during its prime mission were to: (1) Identify safe landing sites; (2) Locate and characterize potential resources; and (3) Characterize the lunar space radiation environment (Tooley et al., 2010). Over the course of its extended missions, LRO has adopted different orbits to prolong mission lifetime while continuing to enable valuable new science measurements. Hence, LRO is currently in a slightly eccentric polar orbit with periapsis at 60 km altitude near the South Pole and apoapsis at an altitude of 120 km. In order for the LRO mission to achieve its objectives, precise orbit determination of the spacecraft has been critical. Radio tracking from ground stations on Earth is an integral aspect of the orbit determination process (Mazarico et al., 2018). This tracking is

conducted in coherent two-way mode at S-band with uplink at 2091.3967±2.5 MHz and downlink at 2271.2±2.5 MHz (Tooley et al., 2010). These frequencies differ so that uplink and downlink signals do not interfere. The turn-around ratio on the spacecraft is the standard 240/221 (Tooley et al., 2010; Pätzold et al., 2004), which ensures that the frequencies are within the standard ranges permitted for uplink and downlink deep space tracking at S-band.

LRO is not tracked when it is behind the Moon, as viewed from Earth. Typically, observations stop shortly before LRO goes behind the Moon (an ingress occultation) and start shortly after LRO emerges from behind the Moon (an egress occultation). The selected extent of a period of tracking observations ensures that all recorded data are suitable for orbit determination. If the duration of radio tracking observations was extended to encompass the occultation of LRO by the Moon, then data acquired when LRO is behind the Moon would contain only noise, and data acquired when LRO is very close to being occulted by the Moon would be degraded by diffraction effects at the lunar limb. However, if such data were recorded, then they could be analyzed to determine electron densities in the lunar ionosphere.

Observation of egress occultations would require rapid (<1 minute) re-establishment of a coherent two-way radio link upon emergence of the spacecraft from behind the Moon. Although this technical capability has been demonstrated by Cassini (Schinder et al., 2015), doing so on LRO might require substantial operational activity to steer the uplink frequency appropriately. It would be premature to consider this before ingress occultation observations have been successfully demonstrated. Here we concentrate on ingress occultation scenarios.

In the orbit determination process, time series of received frequency measurements are used with an existing high-quality lunar gravity field model that is based on GRAIL observations (Zuber et al., 2013) to determine the LRO trajectory (Mazarico et al., 2018). The main ground station used to track LRO is the 18m NASA White Sands (WS1; identifier 119) antenna in New Mexico, USA. This station regularly tracks LRO for 8–10 hours per day (Mazarico et al., 2018). At the time of writing, LRO is also tracked by the Deep Space Network (DSN) for one orbit per day.

The quality of the reconstructed trajectory is expressed in terms of the residuals between the observed and reconstructed range-rate between the ground station and the spacecraft. The characteristic value of range-rate residuals from the WS1 antenna is 0.2 mm $s^{-1}$ (Mazarico et al., 2018). Using the standard Doppler relationship $\Delta f/f = v/c$ (e.g., Withers et al., 2014, and references therein), where $\Delta f$ is the frequency residual, $f$ is an S-band frequency, $v$ is the range-rate residual, and $c$ is the speed of light, this is equivalent to a frequency residual on the order of 1 mHz or a relative frequency accuracy on the order of $10^{-12}$.

The accuracy of radio occultation observations of this quality can be estimated using Equation 1 (Equation 38 of Withers, 2010).

$$\sigma_{Ne} \approx \frac{4\pi\sigma_{\Delta f} f c m_e \epsilon_0}{V e^2} \sqrt{\frac{2\pi H_p}{R}} \tag{1}$$

where $\sigma_{Ne}$ is the uncertainty in inferred electron density, $\sigma_{\Delta f}$ is the uncertainty in the frequency residual, $f$ is the radio frequency, $c$ is the speed of light, $m_e$ is the electron mass, $\epsilon_0$ is the permittivity of free space, $V$ is a component of the spacecraft velocity relative to the Moon (as discussed in Appendix A of

Withers et al. (2014), $V$ is not a speed), $e$ is the elementary charge, $H_p$ is the electron density scale height (also called the plasma scale height), and $R$ is the lunar radius.

Direct application of this equation, which is stated for a one-way occultation observation, yields an expected electron density uncertainty of $1.8 \times 10^9$ m$^{-3}$. For the two-way case relevant for LRO, the actual expected electron density is $9 \times 10^8$ m$^{-3}$, half of the one-way estimate (Withers, 2010). This calculation adopted values of frequency uncertainty of 1 mHz, frequency of the nominal downlink frequency, velocity component of 350 m s$^{-1}$, electron density scale height of 15 km (Section 2), and lunar radius of 1740 km. Inspection of Figure 3 shows that the velocity component depends on time. The adopted value of 350 m s$^{-1}$ is representative for the period when the radio signal samples the ionosphere.

Although useful for order-of-magnitude estimates, this method for projection of electron density uncertainties involves a number of simplifying assumptions (Withers, 2010). Therefore we develop more realistic estimates in the following sections of this article.

## 5 Sample LRO residuals

We examined orbit determination residuals from two-way coherent S-band tracking at the WS1 station between 07 March 2019 and 25 March 2019. There were 53 distinct segments of residuals, each containing approximately 600 points at 5-second intervals for an approximate duration of 50 minutes. One segment that had significantly greater noise than the others was discarded,

leaving 52 distinct segments. Several representative time series of residuals are shown in Figure 2. Ideally, as none of these observations were acquired during occultations, each set of residuals should be consistent with sampling from a normal distribution with mean of zero. Yet this is not the case. Systematic behavior is present in all examples shown, often appearing as a low-order polynomial dependence on time.

## 6 Method

In order to assess the projected performance of LRO radio occultation observations of the lunar ionosphere, should such observations be acquired in the future, we process the available LRO residuals as if they were acquired during an occultation. Since these data were not actually acquired during an occultation, they should yield electron density profiles consistent with sampling from a normal distribution with mean of zero. If these synthetic electron density profiles do appear consistent with normally-distributed noise, then the scatter in the derived electron density values indicates the uncertainty in electron density values that could be determined from future LRO radio tracking observations during an occultation. On the other hand, if these synthetic electron density profiles display systematic trends, then such trends would likely also be present in electron density profiles determined from future LRO radio tracking observations during an occultation. Such trends may confound attempts to detect electrons in the lunar ionosphere.

We convert the range-rate residuals ($v$) into frequency residuals ($\Delta f$) using the standard Doppler relationship $\Delta f/f = v/c$, where $f$ is the nominal downlink frequency. In principle, a more sophisticated approach to this conver-

sion should be implemented for the analysis of actual occultation observations (Withers et al., 2014; Withers and Moore, 2020; Withers et al., 2020). However, this basic approach is suitable for our current purpose of a feasibility study.

In order to process the available time series of LRO residuals as if they were acquired during an occultation, we must adjust their time stamps such that they appear to correspond to the time of an occultation. The values of spacecraft position, velocity, etc., that are used to generate electron density profiles from these frequency residuals are determined based on the adjusted times of the frequency residuals, not the actual times. Therefore we artifically shift the time of each segment of residuals such that each segment ends at an Earth received time of 02:55:00 on 14 March 2019 (UTC). This approach ensures that the "ingress occultation" corresponds to the end of a segment of residuals, just as in an actual observation of an ingress occultation. Should any edge-effects associated with the boundaries of a period of tracking observations contribute to systematic errors in residuals, then they would affect our synthetic observations and future actual occultation observations similarly. The selected date of 14 March 2019 corresponds to an ingress occultation at the center of the actual date range during which these non-occultation observations were acquired.

Figure 3 shows the altitude of the "occultation point" for this time period, where the occultation point is the point of closest approach of the spacecraft-Earth ray path to the center of the Moon. More precisely, it is the point of closest approach of an infinite extension of the spacecraft-Earth ray path to the center of the Moon (see Figure 1). When the spacecraft is on the near-side of the Moon, the ray path does not pass through the ionosphere and the true closest approach distance of the ray path is the spacecraft—Moon distance,

not the (smaller) radial distance of the stated occultation point. When the spacecraft is on the far-side of the Moon, the stated occultation point is an accurate representation of the closest approach of the spacecraft-Earth ray path to the center of the Moon. In Figure 3, the spacecraft moves from the near-side to the far-side at the time of maximum occultation point altitude.

Based on Figures 1 and 3, each set of residuals can be divided into three parts. In the first part, the spacecraft is on the near-side of the Moon and the stated occultation point altitude is not directly applicable to the actual ray path. This corresponds to early times (times less than -410 seconds in Figure 3). In the second part, the spacecraft is on the far-side of the Moon and the occultation point altitude is 50–120 km. Here the ray path passes above the region where ionospheric electrons are expected. This corresponds to intermediate times (-410 to -85 seconds in Figure 3). In the third part, the spacecraft is on the far-side of the Moon and the occultation point altitude is 0–50 km. Here the ray path passes through the region where ionospheric electrons are expected. This corresponds to late times (-85 to 0 seconds in Figure 3). In this example, the radio signal samples the lunar ionosphere for less than two minutes. This duration will change as the occultation geometry changes due to precession of the LRO orbit plane over time.

Based on the earlier results of Ando et al. (2012) and Imamura et al. (2012), we adopt 50 km as the expected upper boundary of the region where appreciable electron densities may occur. In an exponential model of the lunar ionosphere with scale height of 15 km, an altitude of 50 km is more than three scale heights above the region of greatest electron densities. Electron densities would be a factor of 20 smaller at 50 km than at the surface. Given the challenges of merely detecting ionospheric electrons at the Moon, it is reasonable to assert

that densities can be expected to be negligible above 50 km altitude.

Determination of the electron density profile can use only the second and third parts of the residuals, which correspond to when the spacecraft is on the far-side of the Moon and the occultation point altitude decreases monotonically with increasing time (e.g., Withers et al., 2014, and references therein). The second part provides a high-altitude baseline that can be used to characterize experimental performance and the third part provides sampling of the region where ionospheric electrons are expected.

However, results are poor if these parts of the residuals are processed directly without additional preparation. We would expect values in the second part of the residuals to be randomly distributed about a mean value of zero. In these synthetic occultations, that is because these data were acquired at times when the spacecraft was on the lunar near-side and the ray path never encountered the ionosphere. In an actual occultation, that would be because the occultation point altitude is 50–120 km, above the ionosphere.

However, due to the systematic trends apparent in Figure 2, the residuals do not behave in this expected way. Small errors in the orbit determination are responsible for these trends. A mHz error in the Doppler shift of a GHz radio signal is equivalent to an error in spacecraft velocity of $<1$ mm s$^{-1}$. Consequently, derived electron densities at 50–120 km altitude will differ systematically from zero if no additional preparation is applied to the frequency residuals. This is a common phenomenon in radio occultation investigations (e.g., Kliore et al., 1972; Dalba and Withers, 2019; Withers and Moore, 2020; Withers et al., 2020). The common solution is to apply a baseline correction to the frequency residuals to eliminate any such systematic structure.

For these observations, we perform a simple linear baseline correction. We discard the first part of the residuals, then fit the second part of the residuals (50–120 km) to a linear function of time. We subtract that baseline fit from the second and third parts of the residuals (0–120 km) to yield the final residuals. Several representative time series of final frequency residuals are shown in Figure 4. More sophisticated approaches are also possible, such as extending the baseline period to earlier times or fitting to a higher-order polynomial function of time.

Electron density profiles were determined from final residuals using the method adopted for analysis of residuals from similar MAVEN ROSE coherent two-way radio occultation observations at X-band (∼8 GHz) (Withers et al., 2018; Withers and Moore, 2020; Withers et al., 2020).

## 7 Results

We now generate synthetic electron density profiles using the time-shifted corrected frequency residuals. As these residuals were acquired when the ray path did not pass through the lunar ionosphere, we expect the derived electron density profiles to be consistent with zero. Deviations from zero, and any structure present in those deviations, indicate the projected quality of the electron density profiles that would be obtained if suitable LRO observations were acquired during an actual occultation.

Figure 5 shows several representative electron density profiles derived from our time-shifted final residuals. The root-mean-square values of the electron densities in the four profiles shown are $2.5 \times 10^8$ m$^{-3}$, $2.7 \times 10^8$ m$^{-3}$, $1.9 \times 10^8$ m$^{-3}$,

and $1.4 \times 10^8$ m$^{-3}$. These values indicate the electron density uncertainty in each profile. As discussed in Section 5, there are 52 distinct segments of residuals. Each of these segments provided an electron density profile from which a root-mean-square value was determined. The average of the 52 root-mean-square values of the electron density is $2.8 \times 10^8$ m$^{-3}$ and the corresponding standard deviation is $1.2 \times 10^8$ m$^{-3}$.

All derived electron density values from the 52 profiles are shown in Figure 6. A slight bias towards positive values can be seen. This is confirmed by Figure 7, which shows the mean and standard deviation of the 52 derived electron density values at each altitude. The average of all derived electron density values is less than $3 \times 10^7$ m$^{-3}$. At any altitude, the standard deviation in a set of electron density values is on the order of $3 \times 10^8$ m$^{-3}$. However, the standard deviation is clearly influenced by altitude. It decreases from approximately $4 \times 10^8$ m$^{-3}$ at high altitudes to approximately $1 \times 10^8$ m$^{-3}$ at intermediate altitudes, then increases again to approximately $5 \times 10^8$ m$^{-3}$ at low altitudes. We have not developed a convincing explanation for this behavior, a question that we defer to future work. For the exploratory purposes of the present article, a single characteristic value for electron density uncertainty is sufficient. Figure 7 shows that the appropriate value to be adopted is $3 \times 10^8$ m$^{-3}$.

## 8 Discussion

The characteristic uncertainty in a derived electron density profile is $3 \times 10^8$ m$^{-3}$. As the average value of the near-surface electron density reported for dayside observations by Imamura et al. (2012) was also $3 \times 10^8$ m$^{-3}$, this suggests that an individual profile from LRO is unlikely to reliably detect electrons in

the lunar ionosphere, but that averages of multiple LRO profiles under similar geophysical conditions should be able to reliably detect electrons in the lunar ionosphere. As errors in individual profiles are uncorrelated, an average of ten LRO profiles should be sufficient to reduce the experimental uncertainty such that electron density values of $3 \times 10^8$ m$^{-3}$ can be measured reliably. Note that the apparent bias present in the mean electron density imposes a limit on the improvements that can be achieved by averaging ever-greater numbers of profiles. Given the current limited understanding of the state of the lunar ionosphere, it is not clear over what timescales or lengthscales (latitude, solar zenith angle) the ionospheric electron density profile can be considered sufficiently constant for an average of a set of profiles to represent "similar geophysical conditions". Acquisition of a large set of LRO profiles, followed by exploration of how average profiles vary depending on the temporal or spatial range used to select profiles to be averaged, would provide greater clarity on this point. However, this assessment is complicated by the strong altitude dependence of the electron density uncertainty. The uncertainty increases from approximately $1 \times 10^8$ m$^{-3}$ at 50 km altitude to approximately $5 \times 10^8$ m$^{-3}$ at the surface.

Improvements to the quality of electron density profiles derived from LRO radio occultation observations are possible. First, the methods used for orbit determination could be optimized to reduce systematic trends in frequency residuals. The current methods were developed with a focus on accurate knowledge of spacecraft position. Second, further development of methods for the baseline correction may suggest ways to remove the clearly-visible systematic trends more completely. This could involve fit functions of higher degree than the linear function used here, or this could involve the application of a high-

pass filter to remove variations with a characteristic period longer than would be contributed by electrons within 50 km of the lunar surface.

## 9 Conclusions

LRO radio occultation observations of the lunar ionosphere are technically feasible. To acquire such observations, the duration of routine coherent two-way S-band radio tracking observations at the WS1 station would need to be extended by several minutes to capture ingress occultations. Successful acquisition of egress occultation observations would be more technically demanding. It would be premature to consider this before ingress occultation observations have been successfully demonstrated.

Near-surface values of electron density in the dayside lunar ionosphere sporadically exceed $3 \times 10^8$ m$^{-3}$. However, as such detections occur infrequently, large electron densities are probably spatially localized, episodic, or both. The projected uncertainty in a single electron density measurement from an LRO radio occultation observation, $3 \times 10^8$ m$^{-3}$, is the same as this dayside near-surface electron density. Furthermore, the projected uncertainty is greatest near the surface ($5 \times 10^8$ m$^{-3}$) where electron densities are themselves greatest. These challenges can be mitigated by averaging multiple data points to reduce uncertainties. An individual profile from LRO is unlikely to reliably detect electrons in the lunar ionosphere, but averages of multiple ($\sim$10) LRO profiles under similar geophysical conditions should be able to detect electrons in the lunar ionosphere reliably. However, if large electron densities are caused by meteoroid impacts and are short-lived, then averaging profiles acquired once per orbit (every two hours) would not necessarily be beneficial.

Averaging multiple profiles is a viable approach as many profiles could be obtained by LRO. Due to the steady precession of the plane of LRO's polar, low-altitude orbit, occultations occur on approximately 75% of orbits. Given this factor, a 2-hr orbital period, and 8 hours of tracking from WS1 per day, an observing rate of 6 ingress occultations per day or 2000 per year could be achieved. This compares favorably with the 378 observations reported by Imamura et al. (2012) from the dedicated single-spacecraft experiment on Kaguya/SELENE between November 2007 and June 2009. The large number of observations possible for LRO would be sufficient to permit wide-ranging investigations of spatial and temporal variations in the poorly-understood lunar ionosphere.

In summary, electron density profiles from the lunar ionosphere can be determined from routine LRO radio tracking observations with modest impact on current operations. The current cadence of LRO's radio tracking observations from a single ground station can support a remarkable observing rate of 2000 profiles per year. Analysis of projected electron density uncertainties suggests that ionospheric detections are likely if multiple ($\sim$10) profiles are averaged, but not in individual profiles. Motivated by these findings, we hope to be able to conduct such observations in the near future.

**Acknowledgements**

We acknowledge helpful comments from two reviewers. LRO radio science data are archived at the NASA Planetary Data System (https://pds-geosciences.wustl.edu/missions/lro/).

## References


Ando, H., Imamura, T., Nabatov, A., Futaana, Y., Iwata, T., Hanada, H., Matsumoto, K., Mochizuki, N., Kono, Y., Noda, H., Liu, Q., Oyama, K.-I., Yamamoto, Z., Saito, A., 2012. Dual-spacecraft radio occultation measurement of the electron density near the lunar surface by the SELENE mission. J. Geophys. Res. 117, A08313.

Bauer, S. J., 1996. Limits to a lunar ionosphere. Anzeiger Abt. II, available online at http://www.austriaca.at/0xc1aa5576_0x000221cf.pdf 13, 17–21.

Benson, J., Freeman, J. W., Hills, H. K., 1975. The lunar terminator ionosphere. Lunar and Planetary Science Conference Proceedings 3, 3013–3021.

Catling, D. C., Kasting, J. F., 2017. Atmospheric Evolution on Inhabited and Lifeless Worlds. Cambridge University Press, New York.

Chamberlain, J. W., Hunten, D. M., 1987. Theory of planetary atmospheres, 2nd Edition. Academic Press, New York.

Choudhary, R. K., Ambili, K. M., Choudhury, S., Dhanya, M. B., Bhardwaj, A., 2016. On the origin of the ionosphere at the Moon using results from Chandrayaan-1 S band radio occultation experiment and a photochemical model. Geophys. Res. Lett. 43, 10.

Cravens, T. E., 2004. Physics of solar system plasmas. Cambridge University Press, New York.

Dalba, P. A., Withers, P., 2019. Cassini Radio Occultation Observations of Titan's Ionosphere: The Complete Set of Electron Density Profiles. J. Geophys. Res. 124, 643–660.

Glenar, D. A., Stubbs, T. J., McCoy, J. E., Vondrak, R. R., 2011. A reanalysis of the Apollo light scattering observations, and implications for lunar exospheric dust. Planet. Space Sci. 59, 1695–1707.

Imamura, T., Iwata, T., Yamamoto, Z., Mochizuki, N., Kono, Y., Matsumoto, K., Liu, Q., Noda, H., Hanada, H., Oyama, K., Nabatov, A., Futaana, Y., Saito, A., Ando, H., 2008. Studying the Lunar Ionosphere with SELENE Radio Science Experiment. AGU Fall Meeting Abstracts, P51D–04.

Imamura, T., Nabatov, A., Mochizuki, N., Iwata, T., Hanada, H., Matsumoto, K., Noda, H., Kono, Y., Liu, Q., Futaana, Y., Ando, H., Yamamoto, Z., Oyama, K.-I., Saito, A., 2012. Radio occultation measurement of the electron density near the lunar surface using a subsatellite on the SELENE mission. J. Geophys. Res. 117, A06303.

Kliore, A. J., Cain, D. L., Fjeldbo, G., Seidel, B. L., Sykes, M. J., Rasool, S. I., 1972. The atmosphere of Mars from Mariner 9 radio occultation measurements. Icarus 17, 484–516.

Mazarico, E., Neumann, G. A., Barker, M. K., Goossens, S., Smith, D. E., Zuber, M. T., 2018. Orbit determination of the Lunar Reconnaissance Orbiter: Status after seven years. Planet. Space Sci. 162, 2–19.

McCoy, J. E., 1976. Photometric studies of light scattering above the lunar terminator from Apollo solar corona photography. Proceedings of the 7th Lunar and Planetary Science Conference, 1087–1112.

Pätzold, M., Neubauer, F. M., Carone, L., Hagermann, A., Stanzel, C., Häusler, B., Remus, S., Selle, J., Hagl, D., Hinson, D. P., Simpson, R. A., Tyler, G. L., Asmar, S. W., Axford, W. I., Hagfors, T., Barriot, J.-P., Cerisier, J.-C., Imamura, T., Oyama, K.-I., Janle, P., Kirchengast, G., Dehant, V., 2004. MaRS: Mars Express Orbiter Radio Science. ESA SP-1240: Mars Express: the Scientific Payload, available online at http://sci.esa.int/science-e/www/object/index.cfm?fobjectid=34885, pp. 141–163.

Phipps, P. H., Withers, P., Buccino, D. R., Yang, Y.-M., 2018. Distribution of

Plasma in the Io Plasma Torus as Seen by Radio Occultation During Juno Perijove 1. J. Geophys. Res. 123, 6207–6222.

Pluchino, S., Schillirò, F., Salerno, E., Pupillo, G., Maccaferri, G., Cassaro, P., 2008. Radio occultation measurements of the lunar ionosphere. Memorie della Societa Astronomica Italiana Supplementi 12, 53–59.

Reasoner, D. L., Burke, W. J., 1972. Direct Measurement of the Lunar Photoelectron Layer. In: Lunar and Planetary Science Conference. Vol. 3 of Lunar and Planetary Science Conference. pp. 635–636.

Reasoner, D. L., O'Brien, B. J., 1972. Measurement on the lunar surface of impact-produced plasma clouds. J. Geophys. Res. 77 (7), 1292–1299.

Savich, N. A., 1976. Cislunar plasma model. Space Res. 16, 941–943.

Schinder, P. J., Flasar, F. M., Marouf, E. A., French, R. G., Anabtawi, A., Barbinis, E., Kliore, A. J., 2015. A numerical technique for two-way radio occultations by oblate axisymmetric atmospheres with zonal winds. Radio Science 50, 712–727.

Stern, S. A., 1999. The lunar atmosphere: History, status, current problems, and context. Reviews of Geophysics 37, 453–492.

Stubbs, T. J., 2018. Lunar ionosphere. Encyclopedia of Lunar Science, Edited by Brian Cudnik. Springer International Publishing. ISBN 978-3-319-05546-6.

Stubbs, T. J., Glenar, D. A., Farrell, W. M., Vondrak, R. R., Collier, M. R., Halekas, J. S., Delory, G. T., 2011. On the role of dust in the lunar ionosphere. Planet. Space Sci. 59, 1659–1664.

Tooley, C. R., Houghton, M. B., Saylor, R. S., Peddie, C., Everett, D. F., Baker, C. L., Safdie, K. N., 2010. Lunar Reconnaissance Orbiter Mission and Spacecraft Design. Space Sci. Rev. 150, 23–62.

Vasilev, M. B., Vinogradov, V. A., Vyshlov, A. S., Ivanovskii, O. G., Kolosov,

M. A., Savich, N. A., Samovol, V. A., Samoznaev, L. N., Sidorenko, A. I., Sheikhet, A. I., Shtern, D. Y., 1974. Radio Transparency of Circumlunar Space Using the Luna-19 Station. Cosmic Research 12, 102–107.

Vondrak, R. R., 1992. Lunar Base Activities and the Lunar Environment. In: Mendell, W. W., Alred, J. W., Bell, L. S., Cintala, M. J., Crabb, T. M., Durrett, R. H., Finney, B. R., Franklin, H. A., French, J. R., Greenberg, J. S. (Eds.), Lunar Bases and Space Activities of the 21st Century. pp. 337–345.

Vyshlov, A. S., 1976. Preliminary results of circumlunar plasma research by the Luna 22 spacecraft. Space Res. 16, 945–949.

Withers, P., 2010. Prediction of uncertainties in atmospheric properties measured by radio occultation experiments. Advances in Space Research 46, 58–73.

Withers, P., Felici, M., Mendillo, M., Moore, L., Narvaez, C., Vogt, M. F., Jakosky, B. M., 2018. First Ionospheric Results From the MAVEN Radio Occultation Science Experiment (ROSE). J. Geophys. Res. 123, 4171–4180.

Withers, P., Felici, M., Mendillo, M., Moore, L., Narvaez, C., Vogt, M. F., Oudrhiri, K., Kahan, D., Jakosky, B. M., 2020. The MAVEN Radio Occultation Science Experiment (ROSE). Space Sci. Rev. 216 (4), 61.

Withers, P., Moore, L., 2020. How to process radio occultation data: 2. From time series of two-way, single-frequency frequency residuals to vertical profiles of ionospheric properties. Radio Science 55, e2019RS007046.

Withers, P., Moore, L., Cahoy, K., Beerer, I., 2014. How to process radio occultation data: 1. From time series of frequency residuals to vertical profiles of atmospheric and ionospheric properties. Planet. Space Sci. 101, 77–88.

Zuber, M. T., Smith, D. E., Watkins, M. M., Asmar, S. W., Konopliv, A. S., Lemoine, F. G., Melosh, H. J., Neumann, G. A., Phillips, R. J., Solomon,

S. C., Wieczorek, M. A., Williams, J. G., Goossens, S. J., Kruizinga, G., Mazarico, E., Park, R. S., Yuan, D.-N., 2013. Gravity field of the Moon from the Gravity Recovery and Interior Laboratory (GRAIL) mission. Science 339 (6120), 668–671.

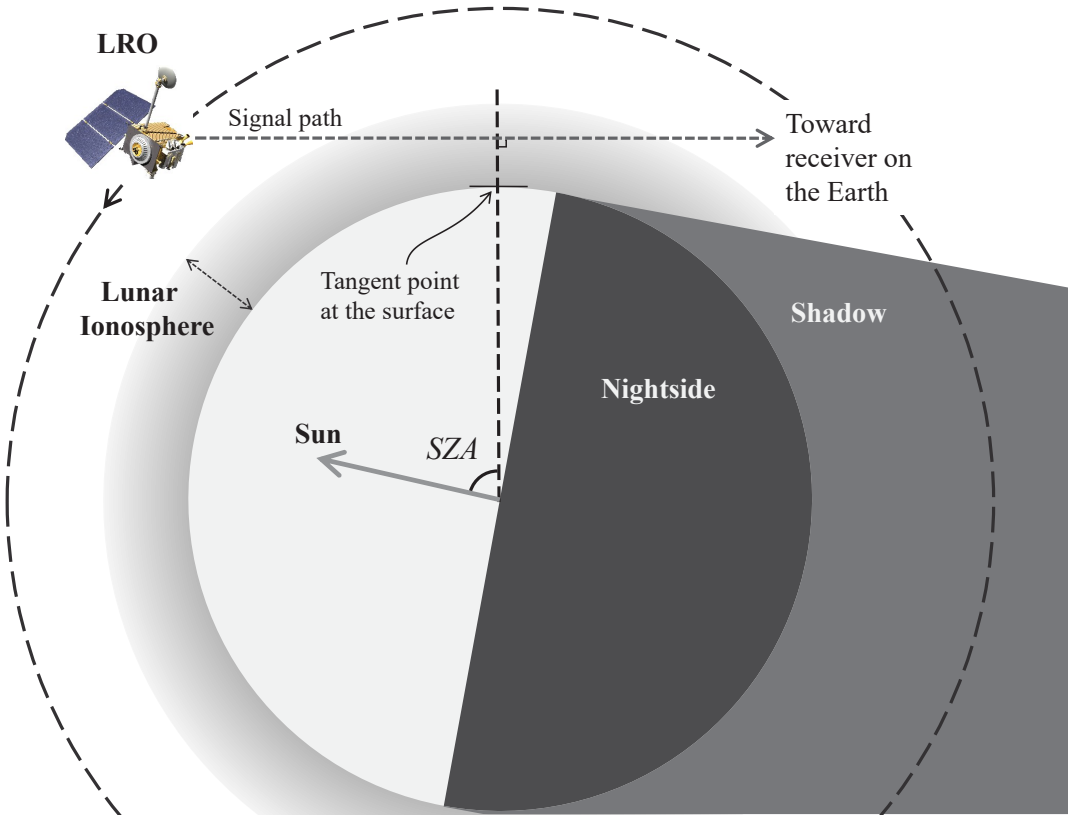


Fig. 1. Illustration of occultation geometry. SZA is solar zenith angle. LRO occultations are not limited to the near-terminator location illustrated here.

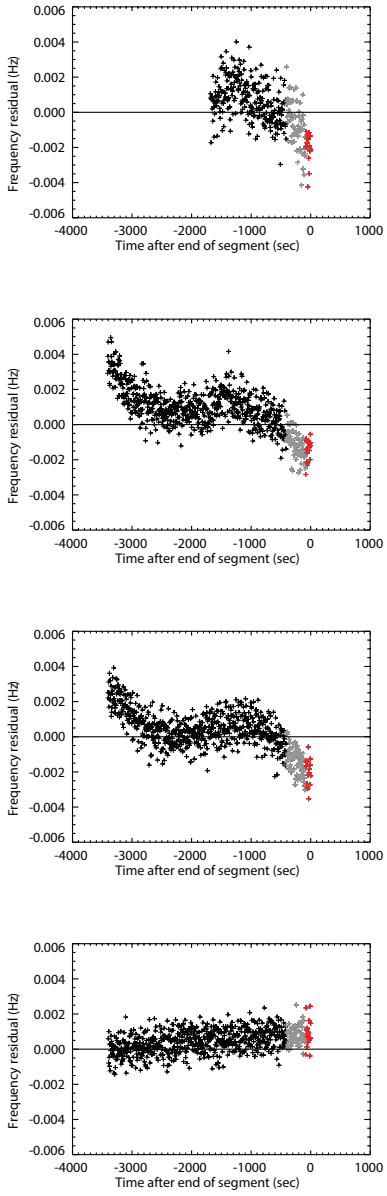


Fig. 2. Time series of original frequency residuals. The horizontal black line indicates zero. Colors are used for consistency with Figure 4. First row. Segment ending at 20:26:15 on 14 March 2019. Second row. Segment ending at 22:23:15 on 14 March 2019. Third row. Segment ending at 02:17:20 on 15 March 2019. Fourth row. Segment ending at 01:05:55 on 17 March 2019.

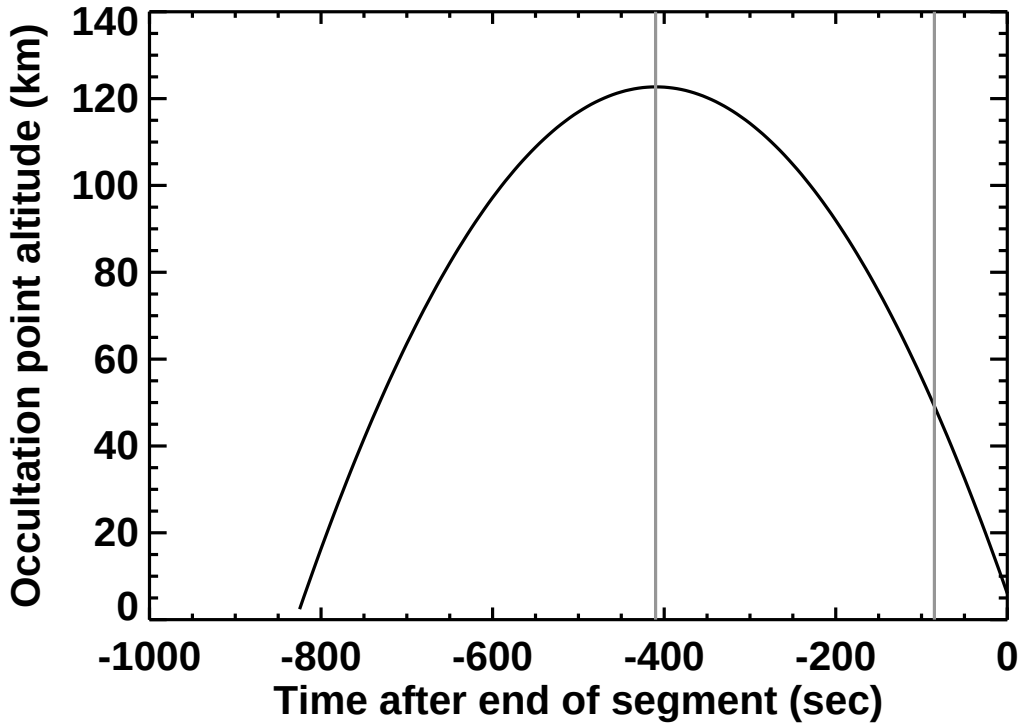


Fig. 3. The black line shows the time series of occultation point altitude, which is defined relative to a sphere of radius 1740 km. The two vertical grey lines define three parts of a time series of frequency residuals. At times earlier than -410 seconds, the spacecraft is on the near-side of the Moon and the stated occultation point altitude is not directly applicable to the actual ray path. At times between -410 seconds and -85 seconds, the spacecraft is on the far-side of the Moon and the occultation point altitude is 50–120 km. Here the ray path passes above the region where ionospheric electrons are expected. At times later than -85 seconds, the spacecraft is on the far-side of the Moon and the occultation point altitude is 0–50 km. Here the ray path passes through the region where ionospheric electrons are expected.

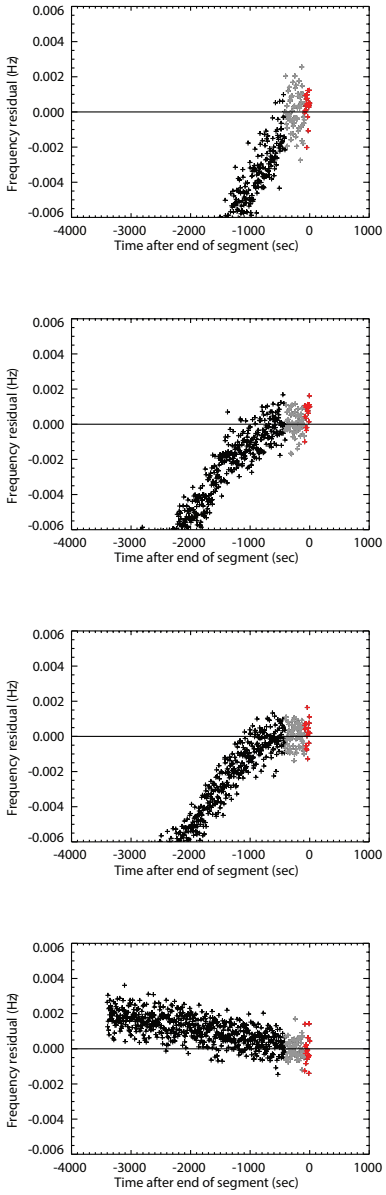


Fig. 4. Time series of corrected frequency residuals. Black symbols are not used in the baseline fit, nor are they used in the generation of the electron density profile (first part of the residuals). Grey symbols correspond to occultation point altitudes of 50–120 km. They are used in the baseline fit and are used in the generation of the electron density profile. Red symbols correspond to occultation point altitudes of 0–50 km. They are not used in the baseline fit, but they are used in the generation of the electron density profile. The horizontal black line indicates zero. First row. Segment ending at 20:26:15 on 14 March 2019. Second row. Segment ending at 22:23:15 on 14 March 2019. Third row. Segment ending at 02:17:20 on 15 March 2019. Fourth row. Segment ending at 01:05:55 on 17 March 2019.

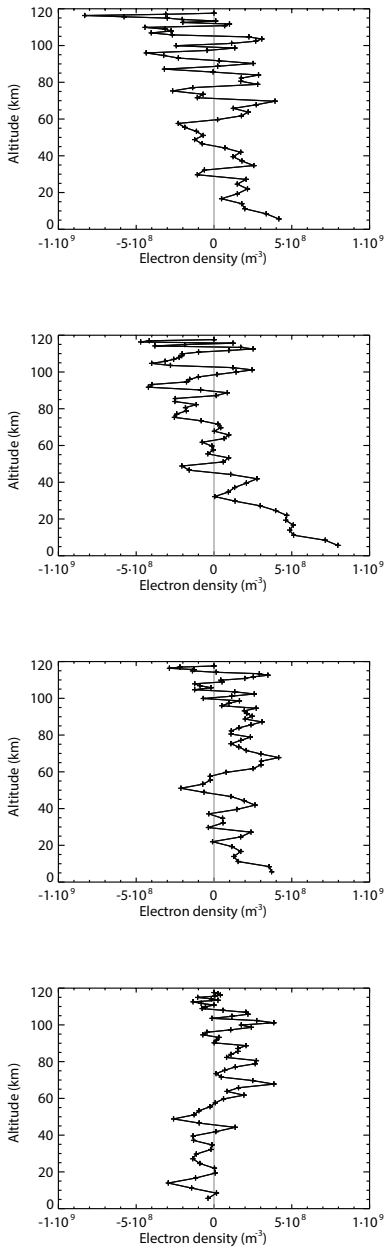


Fig. 5. Derived electron density profiles. The vertical grey line indicates zero. First row. Segment ending at 20:26:15 on 14 March 2019. Second row. Segment ending at 22:23:15 on 14 March 2019. Third row. Segment ending at 02:17:20 on 15 March 2019. Fourth row. Segment ending at 01:05:55 on 17 March 2019.

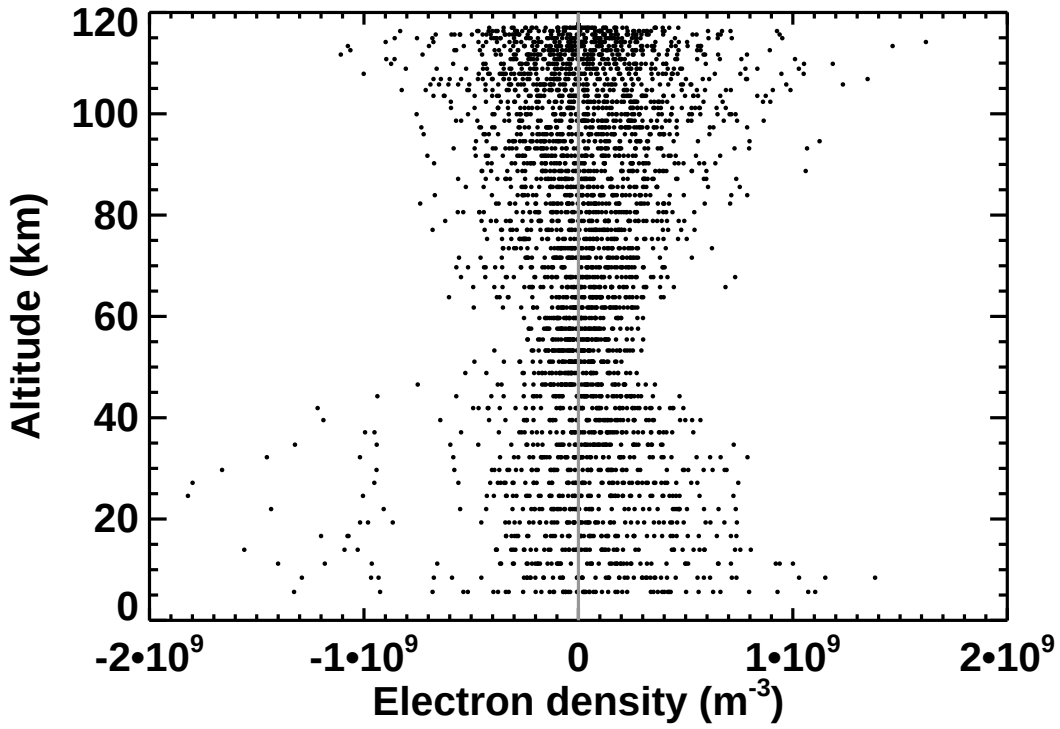


Fig. 6. All derived electron density values from the 52 segments of residuals. The vertical grey line indicates zero.

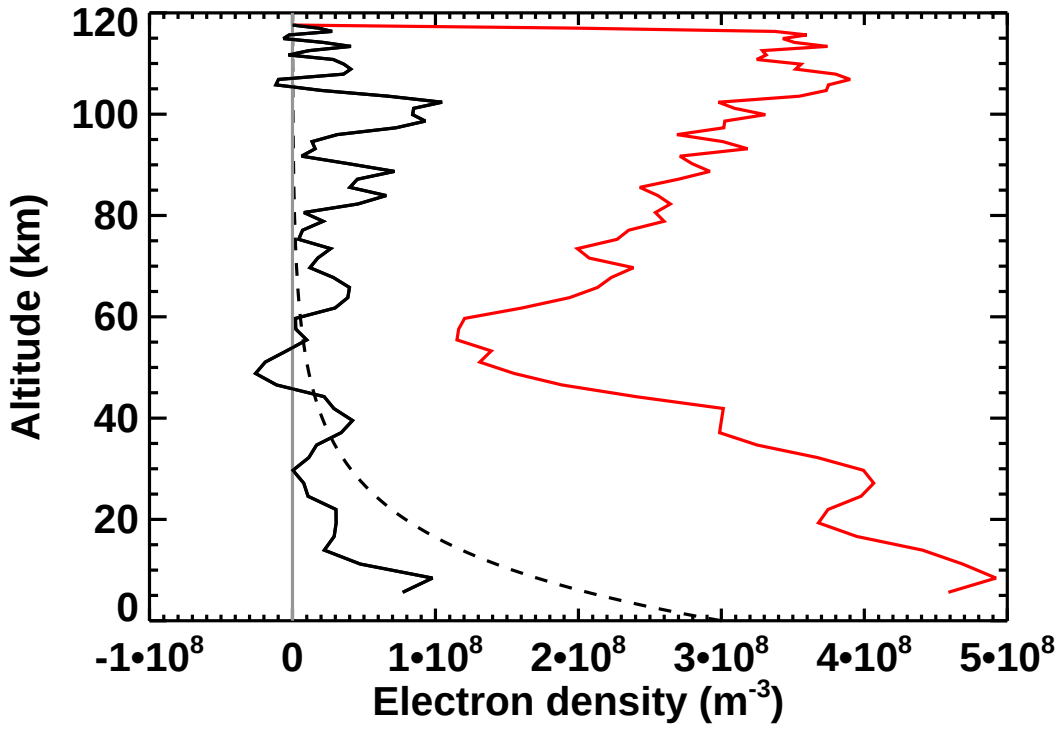


Fig. 7. Mean (black) and standard deviation (red) of the 52 derived electron density values at each altitude. The dashed line is an exponential ionosphere with electron density of $3 \times 10^8$ m$^{-3}$ at the surface and scale height of 15 km. The vertical grey line indicates zero.